

See discussions, stats, and author profiles for this publication at: <https://www.researchgate.net/publication/389170291>

# Structural differences in the outer membrane-associated flagellar rings between sheathed and unsheathed flagella

Article in FEBS Letters · February 2025

DOI: 10.1002/1873-3468.70011

---

CITATIONS

0

READS

21

5 authors, including:



Przemysław Dutka

Genentech

41 PUBLICATIONS 642 CITATIONS

[SEE PROFILE](#)



Tengfei Zhong

University of Chicago

13 PUBLICATIONS 381 CITATIONS

[SEE PROFILE](#)

# Structural differences in the outer membrane-associated flagellar rings between sheathed and unsheathed flagella

 Przemysław Dutka<sup>1,\*</sup>, Ethan H. Li<sup>2</sup>, Tengfei Zhong<sup>2</sup>, Grant J. Jensen<sup>3</sup> and Mohammed Kaplan<sup>2</sup> 
<sup>1</sup> Division of Biology and Biological Engineering, California Institute of Technology, Pasadena, CA, USA

<sup>2</sup> Department of Microbiology, University of Chicago, IL, USA

<sup>3</sup> Department of Chemistry and Biochemistry, Brigham Young University, Provo, UT, USA

**Correspondence**

M. Kaplan, Department of Microbiology, University of Chicago, Chicago, IL 60637, USA

Tel: +7737029743

 E-mail: [mohammedk@uchicago.edu](mailto:mohammedk@uchicago.edu)
**Present address**

\*Department of Structural Biology, Genentech Inc., South San Francisco, CA, USA

(Received 22 March 2024, revised 14 January 2025, accepted 16 January 2025)

doi:10.1002/1873-3468.70011

Edited by Dietmar J. Manstein

The bacterial flagellar motor generates a torque to move the bacterium in its environment. Despite sharing a conserved core, flagellar motors of different species exhibit structural diversity with species-specific embellishments. These embellishments are classified into various types, including integrated (spanning the whole periplasmic space) or outer membrane (OM)-associated ones. Here, we used cryo-electron tomography to investigate the structural differences between the embellishments of sheathed and unsheathed flagella in various species. We discovered that the integrated embellishments of sheathed flagella have disks and rings with a constant diameter, while those of unsheathed flagella have components that vary significantly in diameter. Both unsheathed and sheathed flagella with OM-associated embellishments have components with constant diameter with a subset of motors having an additional extracellular ring. In this Hypothesis article, we propose that these differences may play a role in the formation of the sheath, as having large protein disks of various diameters underneath the OM may interfere with membrane bending to form the sheath.

**Keywords:** bacterial flagellar motor; bacterial motility; cryo-electron tomography; sheathed flagella; structural diversity

The bacterial flagellum is one of the major motility nanomachines in the bacterial domain of life. Structurally, it consists of a long extracellular filament, and a flexible extracellular universal joint known as the hook that connects the filament to a cell-envelope embedded motor [1]. To move the cell, the motor rotates to generate a torque that is transferred through the hook to spin the filament and move the cell in a propeller-like fashion. The motor itself comprises a series of rings that include the C-(cytoplasmic) ring, and the MS-(membrane/supramembrane ring) embedded in the cytoplasmic membrane. Built upon the MS-ring and spanning the periplasm is the so-called rod which acts as a driveshaft to transfer the torque to the hook [1]. The rod is surrounded

by two rings known as the P-(peptidoglycan) and L-(lipopolysaccharide) rings that act as bushing during motor rotation and form a relic structure known as the PL-subcomplex after motor disassembly [2–9]. Torque generation involves the interaction of the upper part of the C-ring with inner-membrane-embedded ion channels, known as the stators, that rotate while pumping ions through the inner membrane (IM), which results in C-ring rotation and torque generation [10–14]. Embedded in the MS-ring is a dedicated type III secretion system that secretes flagellar proteins across the inner membrane to enable the assembly of the flagellum [15].

While all known motors share the conserved core described above, which is similar to the flagellar

**Abbreviations**

cryo-ET, cryo-electron tomography; IM, inner membrane; OM, outer membrane.

systems of *Escherichia coli* and *Salmonella enterica*, flagellar motors of different species exhibit a great structural diversity to optimize the motor function for the environmental niche of each species [16–18]. For example, various species that inhabit viscous environments and require high torque to move incorporate different periplasmic embellishments, which consist of various rings and disks that surround the conserved core of the motor, to stabilize the stators and allow the generation of high torque and enable motility [18–21]. Interestingly, it has been recently shown that some of these periplasmic embellishments consist of type IV pili proteins that have been co-opted by the flagellar system to regulate motility by repressing swimming on semi-solid surfaces and help cells to form microcolonies [22]. Moreover, these embellishments act as a flange that support the motor during disentanglement of the rotating flagellar filament from other flagellar filaments [23].

The advent of cryo-electron tomography (Cryo-ET), which enables the investigation of macromolecular complexes at the nanometer resolution in intact hydrated cells [24], has enabled the visualization and classification of these different types of flagellar periplasmic embellishments. For example, some species, like *Vibrio* spp., have OM-associated embellishments, while others like the periplasmic flagella of Spirochaetes have IM-associated ones. On the other hand, some species like *Helicobacter pylori* and *Campylobacter jejuni* are characterized by integrated embellishments that span the periplasm and are associated with both the IM and OM (Fig. 1, for a recent review on the flagellar periplasmic embellishments, see reference [25] and references therein).

In addition to this structural diversity of the motor, flagella can also be classified as sheathed and unsheathed ones, with the sheathed flagella having the OM extending to encapsulate the flagellar hook and filament. Many bacterial species, including some pathogens, such as *Vibrio* spp. and *H. pylori* have sheathed flagella [16,20], and multiple functions have been proposed for the sheath such as escaping the gastric acid environment or avoiding the host immune response (see [26] and references therein). Interestingly, it has also been shown that rotation of sheathed flagella leads to the release of lipopolysaccharide that activates the host immune system instead of circumventing it in the model squid-vibrio symbiosis [27]. Additionally, the biosynthesis mechanism of the sheath is still unknown [26], and the sheath biogenesis process appears to be different in various species. For example, while mutants of *Vibrio cholerae* and *Brucella melitensis* that do not make filaments, still produce

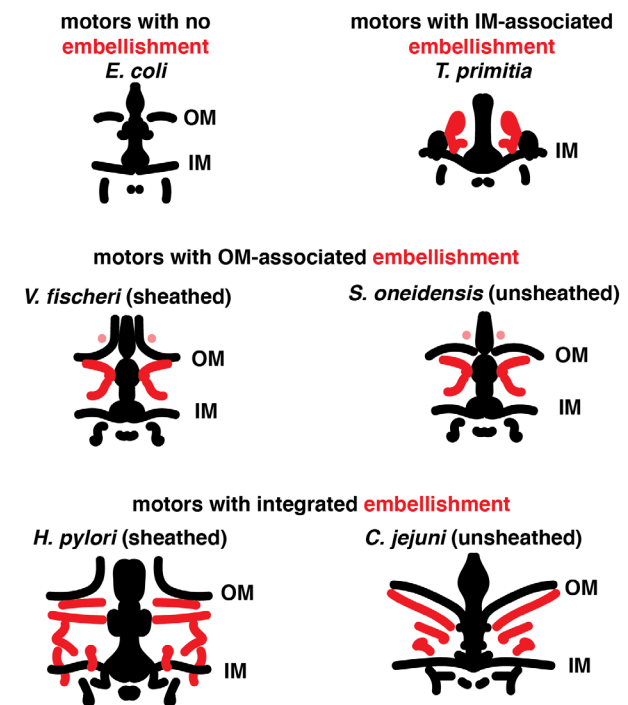


**Fig. 1.** A schematic representation of the different types of embellishments (highlighted in red) present in the bacterial flagellar motors. Note that only a subset of motors with OM-associated embellishments investigated in this study have an extracellular ring (highlighted with transparent red). For more details on flagellar motor embellishments, see reference [25].

empty sheath-like extensions [28,29], sheath biogenesis appears to be coupled to the filament assembly in *H. pylori* [20,30]. On the other hand, *Vibrio alginolyticus* and *Vibrio harveyi* have an extracellular ring, known as the O-ring, located outside the cell, and associated with the sheath base and might be involved in the biogenesis of the sheath in these species [4,31].

Here, we used cryo-ET to investigate the structural differences in the embellishments associated with sheathed and unsheathed flagella. We analyzed tomograms that we previously collected during the course of various projects, in addition to data published in the literature. We found that sheathed flagella with integrated embellishments (*H. pylori*, *Helicobacter hepaticus*, and *Bdellovibrio bacteriovorus*) are characterized by periplasmic disks of a uniform diameter surrounding their PL-rings, and a smaller ring located underneath the OM which remains straight until bending outward. In the unsheathed flagella of *C. jejuni*, *Hydrogenovibrio crunogenus*, and *Wolinella succinogenes*, these embellishments contained disks of variable diameters around the PL-rings, positioned directly beneath the OM which appeared concave. On the other hand, the sheathed and unsheathed flagella with

OM-associated embellishments only, such as the *Vibrio* spp. and *Shewanella oneidensis*, contain disks, which have uniform diameters, surrounding the PL-rings. Interestingly, a subset of flagellar motors in these species (*Vibrio* spp. and *S. oneidensis*) was characterized by an extracellular ring surrounding the sheath. We hypothesize that having embellishments with constant diameter in sheathed flagella is beneficial for bacteria to avoid forming very large disks underneath the OM which could interfere with its outward bending to form the sheath as the presence of large proteinaceous disks directly underneath the OM in unsheathed flagella is correlated with an inward bending of the OM. Moreover, we propose that the rings located directly below or above the OM in sheathed flagella might play a role in the sheath formation in these species.

## Materials and methods

### Strains and growth conditions

*C. jejuni* subspecies *jejuni* 81116 407148 cells were grown under microaerobic conditions for 48–60 h on Mueller–Hinton (MH) agar using CampyPak sachets (Oxoid, Fisher Scientific, Waltham, MA, USA) at 37 °C. Cultures were then restreaked and incubated for additional 16 h. Subsequently, bacteria were resuspended into 1 mL of MH broth to an OD<sub>600</sub> of 10 and were then plunge-frozen. For more detail, see references [4,19]. As for *H. pylori*, a motile revertant *H. pylori* 26695 isolate was selected by serial passage in Brucella broth supplemented with 10% heat-inactivated fetal bovine serum at 37 °C, 5% CO<sub>2</sub> for 4 days until an OD<sub>600</sub>~0.4 was reached (see also references [30,32]). *H. hepaticus* ATCC 51449 cells were grown in standard media as previously reported in [33]. *H. crunogenus* XCL-2 cells were grown in a chemostat with a dilution rate of 0.08 h<sup>-1</sup> in air supplemented with 5% CO<sub>2</sub> as reported in [34–36]. *B. bacteriovorus* attack phase cells were grown in S17-1 prey solution at 30 °C, then filtered by a 0.45 µm filter (for further details see reference [37]). *Vibrio* spp. (*V. cholerae*, *V. harveyi*, *V. fischeri*) were grown as described in reference [4]. *Shewanella oneidensis* cells were grown as detailed in reference [18].

### Cryo-ET sample preparation, imaging, and processing

Cells were mixed with 10- or 20-nm gold beads coated with bovine serum albumin and 4 µL of this mixture was applied to glow-discharged, carbon-coated, R2/2, 200 mesh copper Quantifoil grids (Quantifoil Micro Tools, Jena, Germany) in a Vitrobot chamber (FEI, Thermo Fisher, Waltham, MA, USA) with 100% humidity at room temperature. Sample blotting was done using Whatman paper and subsequently grids were plunge-frozen in an ethane/propane mix. Samples

were imaged using either an FEI Polara 300-keV field emission gun electron microscope (FEI) equipped with a Gatan image filter and K2 Summit direct electron detector in counting mode (Gatan, Pleasanton, CA, USA), or using a Titan Krios 300 keV field emission gun transmission electron microscope (Thermo Fisher Scientific, Waltham, MA, USA) equipped with a Gatan imaging filter and a K2 Summit direct detector in counting mode (Gatan). Data were collected by using the University of California San Francisco (UCSF) Tomography software [38] or SERIALEM software [39] with each tilt series ranging from -60° to 60° and increments of 1° to 3° and an underfocus range of ~ 5 to 10 µm. The following cumulative electron doses were used: 200 e<sup>-</sup>/Å<sup>2</sup> for *C. jejuni*, 130 e<sup>-</sup>/Å<sup>2</sup> for *H. pylori*, 165 e<sup>-</sup>/Å<sup>2</sup> for *H. hepaticus*, 190 e<sup>-</sup>/Å<sup>2</sup> for *H. crunogenus*, 130 e<sup>-</sup>/Å<sup>2</sup> for *B. bacteriovorus*, 160 e<sup>-</sup>/Å<sup>2</sup> for *V. cholerae*, 160 e<sup>-</sup>/Å<sup>2</sup> for *V. harveyi*, 150 e<sup>-</sup>/Å<sup>2</sup> for *V. fischeri*, and 130 e<sup>-</sup>/Å<sup>2</sup> for *S. oneidensis*. After data collection was complete, three-dimensional reconstructions of the obtained tilt series were performed either through the automatic RAPTOR pipeline [40], or manually using the IMOD software package [41].

Statistical analysis and plot visualization were performed using GRAPHPAD PRISM (GraphPad Software, Boston, MA, USA).

## Results

### Flagella with integrated embellishments

To examine and characterize the structural differences between the integrated embellishments of the sheathed and unsheathed flagella, we investigated cryo-tomograms and subtomogram averages of the intact flagellar motors of the unsheathed flagella of *C. jejuni* (EMD-3150), *W. succinogenes* (EMD-3912), and *H. crunogenus*, and the sheathed flagella of *H. pylori* (EMD-8459), *B. bacteriovorus* [37], and *H. hepaticus* (EMD-5299) (Fig. 2). All these species have integrated embellishments spanning the periplasm [16,20,21,36,37]. As described previously [19], the motor of *C. jejuni* is characterized by an integrated scaffold with a large disk, known as the basal disk, surrounding the flagellar PL-rings, and which is formed by FlgP [19] (Fig. 2A). In *H. crunogenus*, which is a Gram-negative bacterium with unsheathed polar flagella, we also identified a large periplasmic disk surrounding the PL-rings (Fig. 2B). To this group of unsheathed flagella, we included the published subtomogram average of *W. succinogenes* motor which is also characterized by an integrated periplasmic embellishment (Fig. 2C, see reference [21]). In the sheathed flagella of *H. pylori*, *H. hepaticus*, and *B. bacteriovorus*, the PL-rings were also surrounded by additional disks and rings (Fig. 2D–F) [16,20]. For consistency,

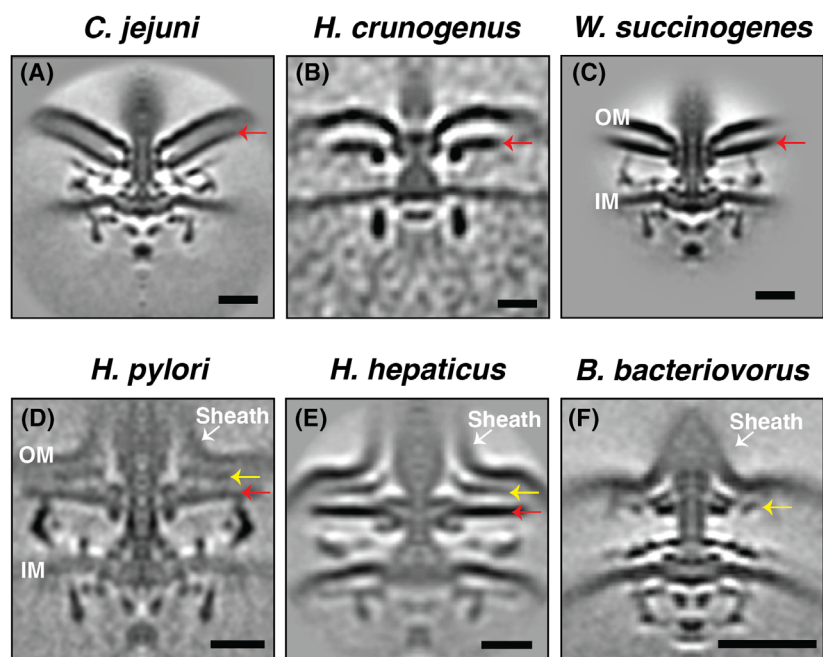


**Fig. 2.** (A–F) Slices through subtomogram averages of the indicated species with the red arrow pointing to the PL-associated disk and the yellow arrow indicating the small ring present directly underneath the OM in sheathed flagella. IM, inner membrane. Scale bar is 20 nm.

we will henceforth refer to all the large disks surrounding the PL-rings in these species (except *B. bacteriovorus*) as the ‘PL-associated disks’ (Fig. 2, red arrows).

While the PL-associated disks of the integrated embellishments in *C. jejuni*, *H. crunogenus*, and *W. succinogenes*, were located directly underneath the OM which appeared concave, an extra smaller ring was present between the corresponding disks and the OM, which appeared straight prior to bending outward to form the sheath, in the sheathed flagella of *H. pylori*, and *H. hepaticus* (Fig. 2D,E, yellow arrows). In *B. bacteriovorus*, only one small ring located underneath the OM was visible in the subtomogram average (Fig. 2F). Moreover, the diameter of the PL-associated disks of the unsheathed flagella varied, unlike those of the sheathed flagella which were more homogenous (Fig. 3). For example, the distance from the P-ring to the edge of the PL-associated disk varied in individual motors from 17 to 55 nm in *C. jejuni* and from 26 to 60 nm in *H. crunogenus* (Fig. 3A–J). While we do not have individual cryo-tomograms of *W. succinogenes* to examine the variations in their PL-disks, previous studies that purified the PL-disk from *W. succinogenes* showed that it has variable diameters, ranging from ~70 to 200 nm [42]. On the other hand, the PL-associated disks of *H. pylori* and *H. hepaticus* had a more consistent diameter of ~31 and ~35 nm in all scrutinized individual motors, respectively (Fig. 3K). Similarly, the additional ring surrounding the PL-rings in *B. bacteriovorus* appeared as a single density and

did not show variation in its diameter and was located ~25 nm from the P-ring in 30 motors.

Subsequently, we examined the correlation between the diameter of the PL-associated disk and the OM inward bending (concavity). All the three motors of unsheathed flagella had their OM bent inwardly (Fig. 2A–C), however, no clear correlation was present between the size of the PL-disk and the degree of bending of the OM in *H. crunogenus*. For this reason, we plotted the curvature angle between the OM and the vertical axis of the motor in *C. jejuni* as the membrane bending was prominent in this species (Fig. 4A, dashed yellow lines). This showed a correlation between the diameter of the PL-associated disk and how much the OM is bent; the larger the disk is, the larger the curvature angle becomes (Fig. 4B). Corroborating this, a motor which has not yet assembled the periplasmic scaffold but only the P- and L-rings, had a flat OM (Fig. 4C). In a motor where only part of the hook is assembled (Fig. 4D), and with a small PL-associated disk (the distance from the P-ring to the edge of the PL-associated disk is ~24 nm), the OM appeared rather bent (Fig. 4D). Interestingly, all the components of the scaffold were already present (the proximal, medial, and basal disks) in this motor (Fig. 4D), while only the proximal end of the hook was present. Similar to what has been previously seen in *Pseudomonas aeruginosa* [3], the tip of the hook was not flat. If this is an assembly stage, then this suggests that the assembly of the hook might not follow a

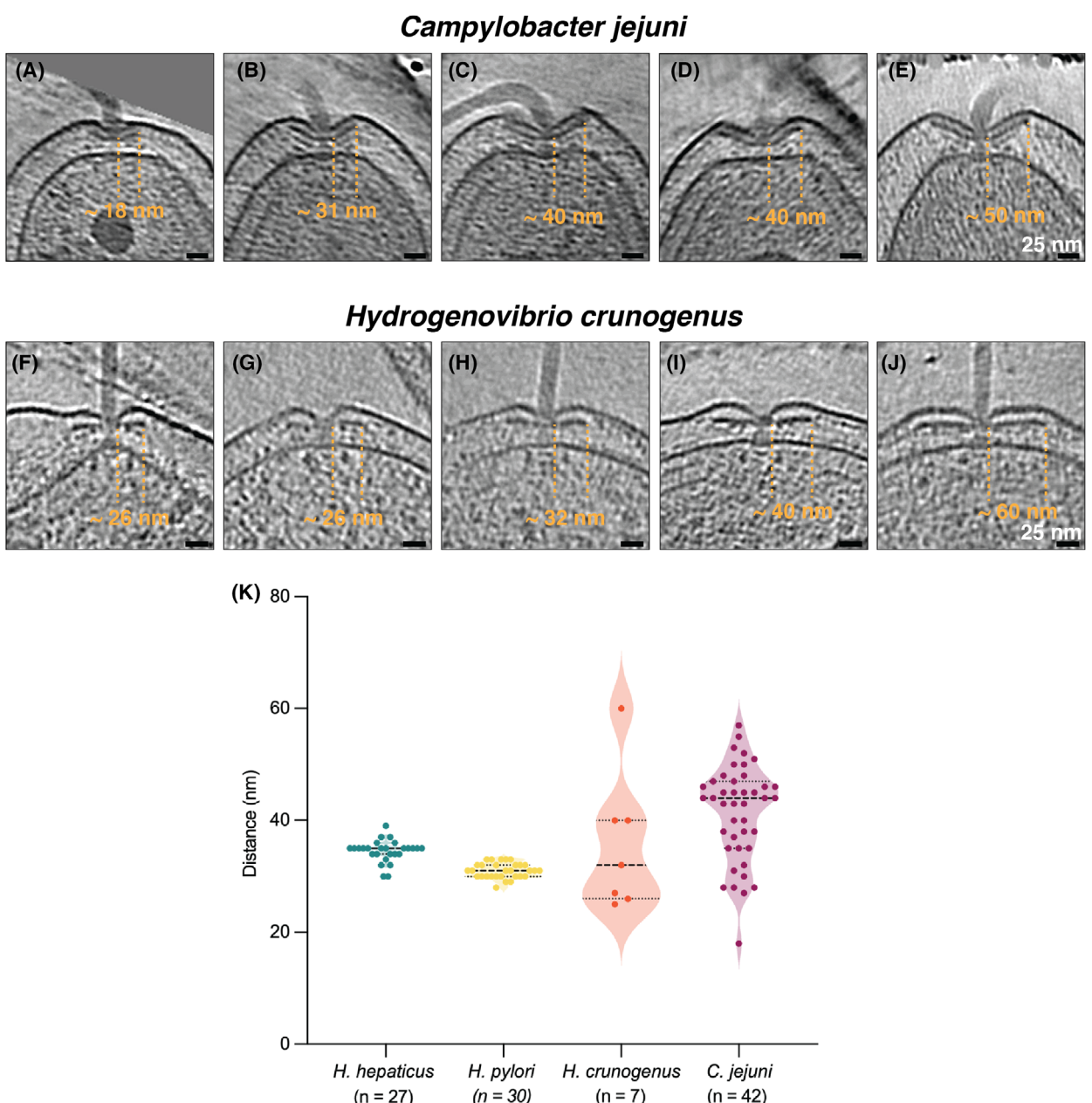


**Fig. 3.** (A–E) Slices through cryo-electron tomograms of *C. jejuni* cells illustrating the presence of flagellar motors having PL-associated disks with variable diameters. The approximate distance from the P-ring to the edge of the disk is indicated. (F–J) Similar to (A–E) but for *H. crunogenus*. Scale bar is 25 nm. (K) Violin plot indicating the approximate distance from the P-ring to the edge of the PL-associated disk in the four species investigated in this study. The number of the examined motors from each species is indicated below the species name on the x-axis. Black dashed center lines indicate medians, and the upper and lower dashed lines denote the interquartile range. Each dot represents an individual measurement.

symmetrical pattern and that the assembly of the scaffold precedes (or concomitant) to the biogenesis of the hook and the filament. However, we cannot exclude that this hook was broken for any reason. As expected, a fully assembled flagellum (where the distance from the P-ring to the edge of the PL-associated

disk was ~45 nm) had a notably bent OM near the exit point of the flagellum (Fig. 4E), compared to the motor with a smaller PL-associated disk (Fig. 4D). In conclusion, sheathed flagella with integrated scaffolds examined here have PL-associated disks with a homogeneous diameter and a smaller ring (or disk) located

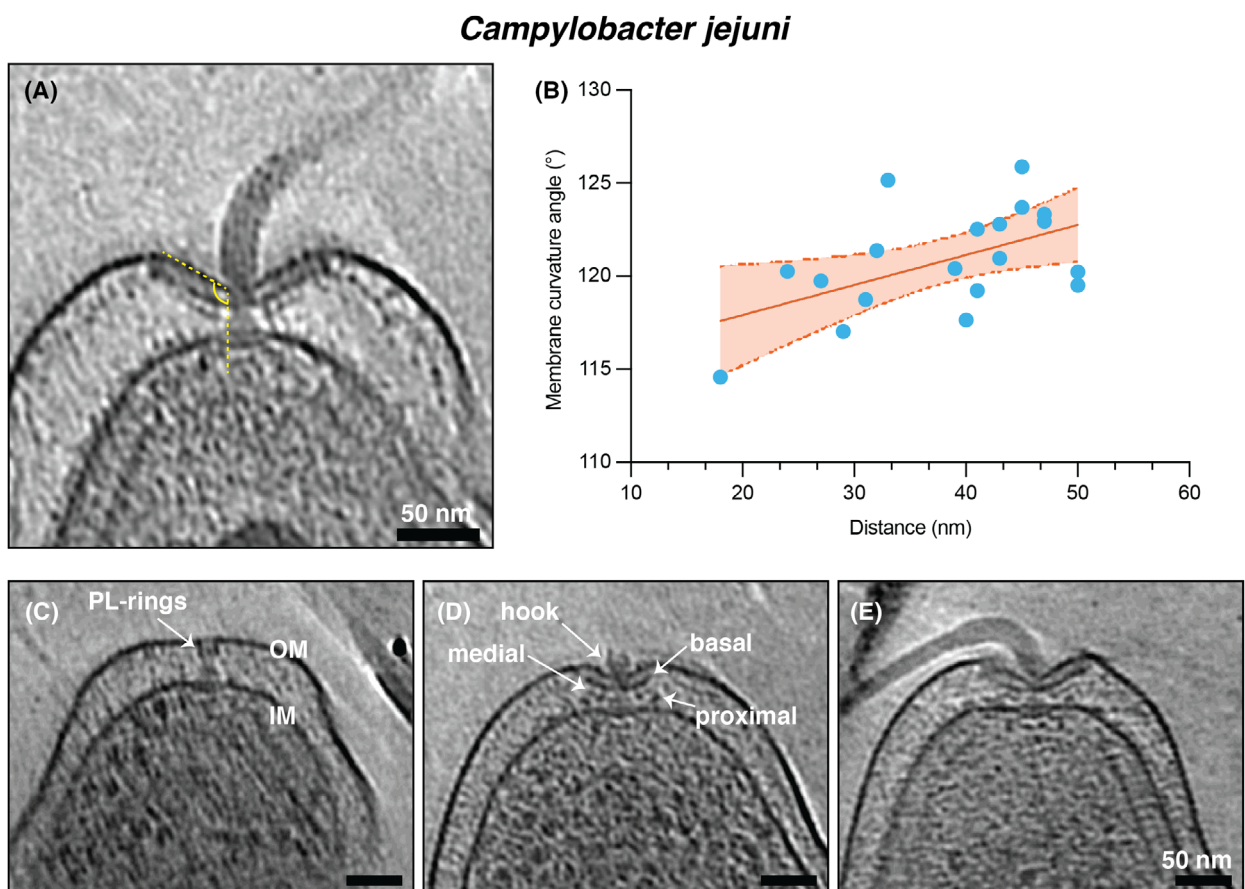


**Fig. 4.** (A) A slice through a cryo-electron tomogram of a *C. jejuni* cell highlighting the inward bending of the OM as indicated by the curvature angle shown in yellow (used for the plot shown in panel B), which is defined as the angle between the OM and the long axis of the motor. (B) Correlation between the curvature angle of the outer membrane and PL-associated disk size. The solid orange line represents a simple linear regression fit and the dashed lines represent a 95% confidence interval. The distance on the x-axis refers to the distance from the P-ring to the edge of the disk. (C–E) Slices through cryo-electron tomograms of *C. jejuni* cells indicating, presumably, motors at different assembly stages without (C) or with (D, E) the PL-associated disk (with various diameters). Panel (C) represents a motor prior to the assembly of the PL-associated disk and with a straight OM. Panels (D and E) show motors with PL-associated disks of different sizes and inward curvature of the OM. Scale bar (panels A, C, D, E) is 50 nm.

directly underneath the OM, while those of unsheathed flagella examined here have disks with significantly variable diameters. In one species (*C. jejuni*), the size of the PL-associated disk correlated with the degree of the inward bending of the OM.

#### Flagella with OM-associated embellishments

We then examined the periplasmic embellishments of the sheathed flagella of *V. cholerae* (EMD-5308), *V. fischeri* (EMD-3155), *V. harveyi* [4], and the unsheathed flagella of *Shewanella oneidensis* (EMD-0467) (Fig. 5). The motors of all these species are characterized by OM-associated embellishments consisting of the so-called H- and T-rings (Fig. 5A–D). Individual

motors of all these four species have H- and T-rings with constant diameters with the distance from the P-ring to the edge of the H-ring was ~16–18 nm, while that to the edge of the T-ring ~10–12 nm (Fig. 5E). Interestingly, we found that a subset of motors in *V. fischeri* (3 out of 24 motors), *V. harveyi* (6 out of 24 motors), and *S. oneidensis* (11 out of 39 motors) have an extracellular ring surrounding the (sheathed) filament (Table 1 and Fig. 5F–K blue arrows). We did not observe this ring in 34 motors of sheathed *V. cholerae* flagella. In conclusion, both sheathed and unsheathed flagella with OM-associated embellishments that we examined here have components of uniform diameters and a subset of the motors have an extracellular ring surrounding the flagellar filament.

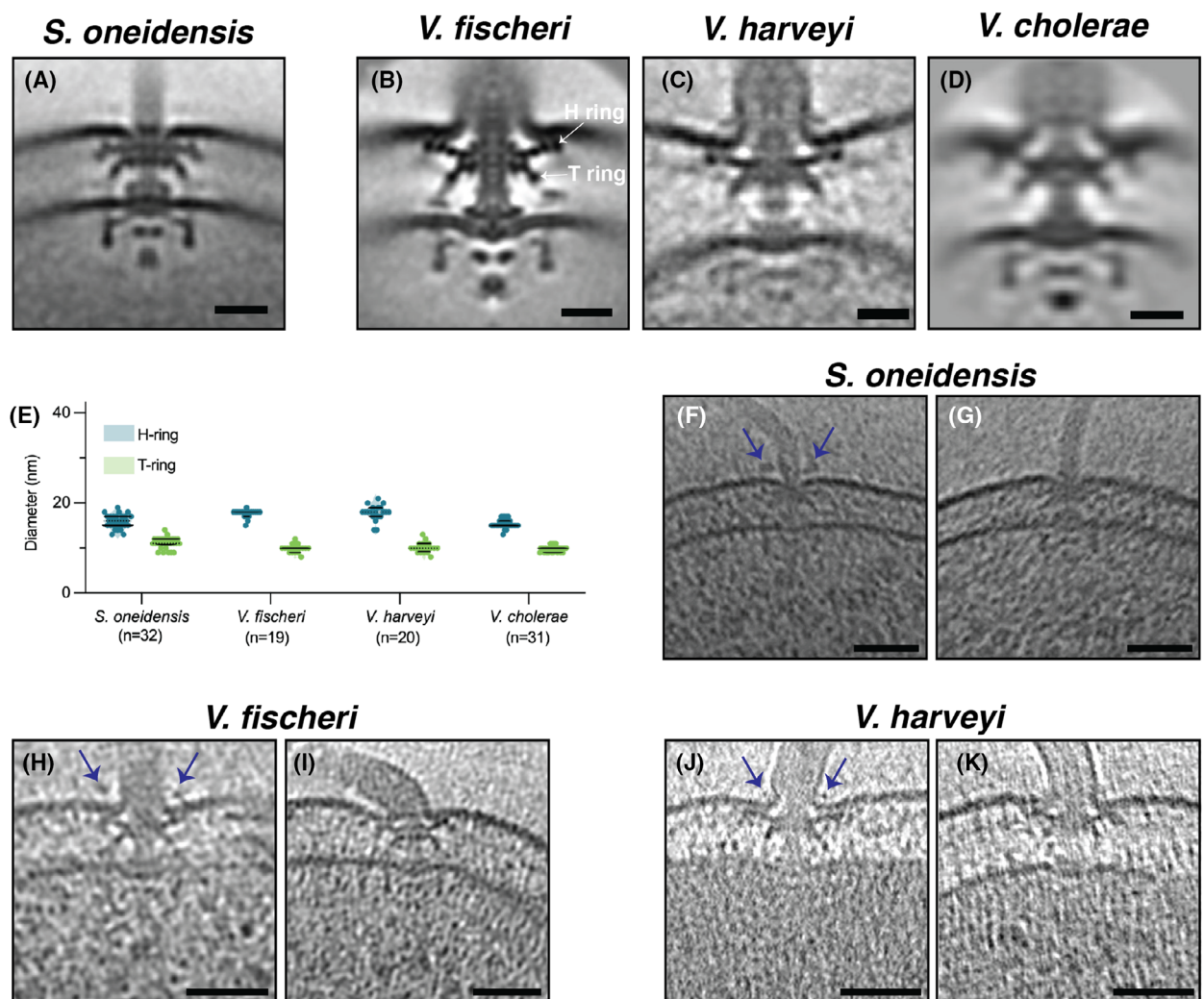


**Fig. 5.** (A–D) Slices through subtomogram averages of the indicated species. The H- and T-rings are highlighted in the *V. fischeri* motor. Scale bar is 20 nm. (E) Violin plot indicating the diameters of the H-ring and T-rings of the four species investigated in this study. The number of the examined motors from each species is indicated below the species name on the x-axis. Black dashed center lines indicate medians, and the upper and lower dashed lines denote the interquartile range. Each dot represents an individual measurement. (F–K) Slices through cryo-electron tomograms of the indicated species highlighting the presence of an extracellular ring in a subset of motors in these species (blue arrows). Scale bar is 50 nm.

## Discussion

To summarize, the PL-associated disks of the examined unsheathed flagella with integrated embellishments had variable diameters and located directly beneath the OM which appeared to bend inward. In *C. jejuni*, this inward bending of the OM was proportionally correlated to the disk diameter. Interestingly, the PL-associated disk in *W. succinogenes* assembles through the polymerization of protein subunits forming an Archimedean spiral and not as concentric rings.

**Table 1.** Number of flagellar motors extracellular rings in various species investigated in this study.

Species	Total number of examined motors	Motors with extracellular ring
<i>Vibrio fischeri</i>	24	3
<i>Vibrio cholerae</i>	34	0
<i>Vibrio harveyi</i>	24	6
<i>Shewanella oneidensis</i>	37	11

However, the corresponding disk in *C. jejuni* assembles as concentric rings of FlgP presumably due to the presence of another protein, PflC, which is not present in *W. succinogenes* [43]. Conversely, the PL-associated disks of the sheathed flagella with integrated embellishments (*H. pylori* and *H. hepaticus*) have a uniform diameter and are separated from the OM by another smaller ring, which is also present in the motor of *B. bacteriovorus*. This smaller ring might act as a ‘buffer ring’ between the OM and the other large periplasmic disks of the flagellar motor, which might interfere with the outward bending of the OM during sheath biogenesis.

The motors of *Vibrio* spp. have periplasmic embellishments consisting of the H- and T-rings which both have constant diameters. In *V. harveyi* and *V. fischeri*, a subset of the motors was associated with an extracellular ring. While we previously reported the presence of an extracellular ring in the motors of *V. harveyi* [4], their presence in the motors of *V. fischeri* is novel. Interestingly, this observation is in accordance with what has been described previously for *V. alginolyticus* where a subset of motors is sheathed and have an extracellular ring surrounding the sheath (referred to as the O-ring), while another subset of flagella is unsheathed and lack the O-ring, suggesting a role for this ring in sheath formation [31]. However, the absence of the H-ring from the sheathed flagellum of *V. alginolyticus* results in unsheathed flagella or periplasmic ones instead of regular sheathed flagella in this species [44] suggesting that the O-ring alone is not enough to form the sheath in *V. alginolyticus*. In our case, both subsets of motors of *V. harveyi* and *V. fischeri* (with and without an extracellular ring) were sheathed. Similar to previous reports [18], an extracellular ring also surrounds a subset of the unsheathed filaments of *S. oneidensis* flagella suggesting that these extracellular rings could have diverse roles other than sheath formation. The fact that the extracellular ring is only associated with a subset of motors in these species might suggest a transient nature for it, like the recently described transient cytoplasmic rings that stabilize the motor during assembly in various species [30]. Similarly, these extracellular rings might dissociate after the sheath formation, but we cannot exclude other reasons. A similar role might be played by the small ring located directly underneath the OM in sheathed flagella with integrated embellishments such as *H. pylori*, *B. bacteriovorus*, and *H. hepaticus*. For this reason, identifying the component(s) of these rings, might shed light on how the sheath is formed, which remains hitherto enigmatic [26].

## Acknowledgements

MK acknowledges funding from the University of Chicago (startup package). GJJ acknowledges funding from NIH grant R01 AI127401.

## Author contributions

MK: designed study, analyzed data, drafted paper, and data generation. GJJ: analyzed data and drafted paper. TZ: drafted paper. EHL: analyzed data. PD: analyzed data, drafted paper, and data generation.

## Peer review

The peer review history for this article is available at <https://www.webofscience.com/api/gateway/wos/peer-review/10.1002/1873-3468.70011>.

## Data accessibility

Subtomogram averages used in this study are available in the Electron Microscopy Data Bank and their accession numbers are indicated in the manuscript. Individual tomograms are available upon request.

## References

- 1 Macnab RM (2003) How bacteria assemble flagella. *Annu Rev Microbiol* **57**, 77–100.
- 2 Ferreira JL, Gao FZ, Rossmann FM, Nans A, Brenzinger S, Hosseini R, Wilson A, Briegel A, Thormann KM, Rosenthal PB et al. (2019)  $\gamma$ -Proteobacteria eject their polar flagella under nutrient depletion, retaining flagellar motor relic structures. *PLoS Biol* **17**, e3000165.
- 3 Kaplan M, Subramanian P, Ghosal D, Oikonomou CM, Pirbadian S, Starwalt-Lee R, Mageswaran SK, Ortega DR, Gralnick JA, El-Naggar MY et al. (2019) *In situ* imaging of the bacterial flagellar motor disassembly and assembly processes. *EMBO J* **38**, e100957.
- 4 Kaplan M, Sweredoski MJ, Rodrigues JPGLM, Tocheva EI, Chang Y-W, Ortega DR, Beeby M and Jensen GJ (2020) Bacterial flagellar motor PL-ring disassembly subcomplexes are widespread and ancient. *Proc Natl Acad Sci U S A* **117**, 201916935.
- 5 Kaplan M, Wang Y, Chreifi G, Zhang L, Chang Y-W and Jensen GJ (2021) Programmed flagellar ejection in *Caulobacter crescentus* leaves PL-subcomplexes. *J Mol Biol* **433**, 167004.
- 6 Zhu S, Schniederberend M, Zhitnitsky D, Jain R, Galán JE, Kazmierczak BI and Liu J (2019) *In situ* structures of polar and lateral flagella revealed by Cryo-electron tomography. *J Bacteriol* **201**, e00117-19.

- 7 Zhu S and Gao B (2020) Bacterial flagella loss under starvation. *Trends Microbiol* **28**, 785–788.
- 8 Zhuang X-Y and Lo C-J (2020) Construction and loss of bacterial Flagellar filaments. *Biomolecules* **10**, 1528.
- 9 Zhuang X, Guo S, Li Z, Zhao Z, Kojima S, Homma M, Wang P, Lo C and Bai F (2020) Live-cell fluorescence imaging reveals dynamic production and loss of bacterial flagella. *Mol Microbiol* **114**, 279–291.
- 10 Chang Y, Zhang K, Carroll BL, Zhao X, Charon NW, Norris SJ, Motaleb MA, Li C and Liu J (2020) Molecular mechanism for rotational switching of the bacterial flagellar motor. *Nat Struct Mol Biol* **27**, 1041–1047.
- 11 Deme JC, Johnson S, Vickery O, Aron A, Monkhouse H, Griffiths T, James RH, Berks BC, Coulton JW, Stansfeld PJ et al. (2020) Structures of the stator complex that drives rotation of the bacterial flagellum. *Nat Microbiol* **5**, 1553–1564.
- 12 Santiveri M, Roa-Eguiara A, Kühne C, Wadhwa N, Hu H, Berg HC, Erhardt M and Taylor NMI (2020) Structure and function of stator units of the bacterial Flagellar motor. *Cell* **183**, 244–257.e16.
- 13 Hu H, Santiveri M, Wadhwa N, Berg HC, Erhardt M and Taylor NMI (2021) Structural basis of torque generation in the bi-directional bacterial flagellar motor. *Trends Biochem Sci* **47**, 160–172.
- 14 Tan J, Zhang X, Wang X, Xu C, Chang S, Wu H, Wang T, Liang H, Gao H, Zhou Y et al. (2021) Structural basis of assembly and torque transmission of the bacterial flagellar motor. *Cell* **184**, 2665–2679.e19.
- 15 Diepold A and Armitage JP (2015) Type III secretion systems: the bacterial flagellum and the injectisome. *Philos Trans R Soc Lond B Biol Sci* **370**, 20150020.
- 16 Chen S, Beeby M, Murphy GE, Leadbetter JR, Hendrixson DR, Briegel A, Li Z, Shi J, Tocheva EI, Müller A et al. (2011) Structural diversity of bacterial flagellar motors: structural diversity of bacterial flagellar motors. *EMBO J* **30**, 2972–2981.
- 17 Zhao X, Norris SJ and Liu J (2014) Molecular architecture of the bacterial Flagellar Motor in Cells. *Biochemistry* **53**, 4323–4333.
- 18 Kaplan M, Ghosal D, Subramanian P, Oikonomou CM, Kjaer A, Pirbadian S, Ortega DR, Briegel A, El-Naggar MY and Jensen GJ (2019) The presence and absence of periplasmic rings in bacterial flagellar motors correlates with stator type. *Elife* **8**, e43487.
- 19 Beeby M, Ribardo DA, Brennan CA, Ruby EG, Jensen GJ and Hendrixson DR (2016) Diverse high-torque bacterial flagellar motors assemble wider stator rings using a conserved protein scaffold. *Proc Natl Acad Sci U S A* **113**, E1917–E1926.
- 20 Qin Z, Lin W, Zhu S, Franco AT and Liu J (2017) Imaging the motility and chemotaxis machineries in helicobacter pylori by Cryo-electron tomography. *J Bacteriol* **199**, e00695-16.
- 21 Chaban B, Coleman I and Beeby M (2018) Evolution of higher torque in campylobacter-type bacterial flagellar motors. *Sci Rep* **8**, 97.
- 22 Liu X, Tachiyama S, Zhou X, Mathias RA, Bonny SQ, Khan MF, Xin Y, Roujeinikova A, Liu J and Ottemann KM (2024) Bacterial flagella hijack type IV pili proteins to control motility. *Proc Natl Acad Sci U S A* **121**, e2317452121.
- 23 Cohen EJ, Drobnić T, Ribardo DA, Yoshioka A, Umrekar T, Guo X, Fernandez J-J, Brock EE, Wilson L, Nakane D et al. (2024) Evolution of a large periplasmic disk in Campylobacterota flagella enables both efficient motility and autoagglutination. *Dev Cell* **59**, 3306–3321.e5.
- 24 Kaplan M, Nicolas WJ, Zhao W, Carter SD, Metskas LA, Chreifi G, Ghosal D and Jensen GJ (2021) In situ imaging and structure determination of biomolecular complexes using electron Cryo-tomography. In cryoEM (Gonen T and Nannenga BL, eds), pp. 83–111. Springer US, New York, NY.
- 25 Zhou X and Roujeinikova A (2021) The structure, composition, and role of periplasmic stator scaffolds in polar bacterial Flagellar motors. *Front Microbiol* **12**, 639490.
- 26 Chu J, Liu J and Hoover TR (2020) Phylogenetic distribution, ultrastructure, and function of bacterial Flagellar sheaths. *Biomolecules* **10**, 363.
- 27 Brennan CA, Hunt JR, Kremer N, Krasity BC, Apicella MA, McFall-Ngai MJ and Ruby EG (2014) A model symbiosis reveals a role for sheathed-flagellum rotation in the release of immunogenic lipopolysaccharide. *Elife* **3**, e01579.
- 28 Richardson K, Nixon L, Mostow P, Kaper JB and Michalski J (1990) Transposon-induced non-motile mutants of *Vibrio cholerae*. *J Gen Microbiol* **136**, 717–725.
- 29 Ferooz J and Letesson J-J (2010) Morphological analysis of the sheathed flagellum of *Brucella melitensis*. *BMC Res Notes* **3**, 333.
- 30 Kaplan M, Oikonomou CM, Wood CR, Chreifi G, Subramanian P, Ortega DR, Chang Y, Beeby M, Shaffer CL and Jensen GJ (2022) Novel transient cytoplasmic rings stabilize assembling bacterial flagellar motors. *EMBO J* **41**, e109523.
- 31 Zhu S, Nishikino T, Hu B, Kojima S, Homma M and Liu J (2017) Molecular architecture of the sheathed polar flagellum in *Vibrio alginolyticus*. *Proc Natl Acad Sci U S A* **114**, 201712489.
- 32 Chang Y-W, Shaffer CL, Rettberg LA, Ghosal D and Jensen GJ (2018) In vivo structures of the *Helicobacter pylori* cag type IV secretion system. *Cell Rep* **23**, 673–681.
- 33 Briegel A, Ortega DR, Tocheva EI, Wuichet K, Li Z, Chen S, Muller A, Iancu CV, Murphy GE, Dobro MJ et al. (2009) Universal architecture of bacterial chemoreceptor arrays. *Proc Natl Acad Sci U S A* **106**, 17181–17186.

- 34 Dobrinski KP, Longo DL and Scott KM (2005) The carbon-concentrating mechanism of the hydrothermal vent Chemolithoautotroph *Thiomicrospira crunogena*. *J Bacteriol* **187**, 5761–5766.
- 35 Iancu CV, Morris DM, Dou Z, Heinhorst S, Cannon GC and Jensen GJ (2010) Organization, structure, and assembly of  $\alpha$ -Carboxysomes determined by electron Cryotomography of intact cells. *J Mol Biol* **396**, 105–117.
- 36 Kaplan M, Tocheva EI, Briegel A, Dobro MJ, Chang Y-W, Subramanian P, McDowall AW, Beeby M and Jensen GJ (2021) Loss of the bacterial Flagellar motor switch complex upon cell lysis. *MBio* **12**, e0029821.
- 37 Kaplan M, Chang Y-W, Oikonomou CM, Nicolas WJ, Jewett AI, Kreida S, Dutka P, Rettberg LA, Maggi S and Jensen GJ (2023) Bdellovibrio predation cycle characterized at nanometre-scale resolution with cryo-electron tomography. *Nat Microbiol* **8**, 1267–1279.
- 38 Zheng SQ, Keszthelyi B, Branolund E, Lyle JM, Braunfeld MB, Sedat JW and Agard DA (2007) UCSF tomography: an integrated software suite for real-time electron microscopic tomographic data collection, alignment, and reconstruction. *J Struct Biol* **157**, 138–147.
- 39 Mastronarde DN (2005) Automated electron microscope tomography using robust prediction of specimen movements. *J Struct Biol* **152**, 36–51.
- 40 Ding HJ, Oikonomou CM and Jensen GJ (2015) The Caltech tomography database and automatic processing pipeline. *J Struct Biol* **192**, 279–286.
- 41 Kremer JR, Mastronarde DN and McIntosh JR (1996) Computer visualization of three-dimensional image data using IMOD. *J Struct Biol* **116**, 71–76.
- 42 Engelhardt H, Schuster SC and Baeuerlein E (1993) An Archimedian spiral: the basal disk of the *Wolinella* Flagellar motor. *Science* **262**, 1046–1048.
- 43 Drobnić T, Cohen EJ, Alzheimer M, Froschauer K, Svensson S, Singh N, Garg SG, Henderson L, Umrekar T, Nans A et al. (2023) Molecular model of a bacterial flagellar motor in situ reveals a “parts-list” of protein adaptations to increase torque. *bioRxiv*. <https://doi.org/10.1101/2023.09.08.556779>.
- 44 Zhu S, Nishikino T, Kojima S, Homma M and Liu J (2018) The *Vibrio* H-ring facilitates the outer membrane penetration of the polar sheathed flagellum. *J Bacteriol* **200**, e00387-18.